

20 **Abstract**

21 The *Arenaviridae* is a large family of viruses causing both acute and persistent infections
22 and causing significant public health concerns in afflicted regions. A “trademark” of infection is the
23 quick and efficient immuno-suppression mediated in part by a 3’-5’ RNA exonuclease domain
24 (ExoN) of the Nucleoprotein (NP). Mopeia virus, the eastern African counterpart of Lassa virus,
25 carries such ExoN domain, but does not suppress the host innate immunity. We have recently
26 reported the crystal structure of the Mopeia virus ExoN domain, which presents a conserved fold
27 and active site. In the present study, we show that the ExoN activity rules out a direct link between
28 ExoN activity and alteration of the host innate immunity. We found that the Arenavirus ExoN,
29 however, is able to excise mis-incorporated bases present at the 3’-end of double stranded RNA.
30 ExoN(-) arenaviruses cultured in cells dampened in innate immunity still replicated in spite of a
31 significant reduction in the viral charge over several passages. The remaining ExoN(-) virus
32 population showed an increased base substitution rate on a narrow nucleotide spectrum, linking the
33 ExoN activity to genome editing. Since, the Arenavirus ExoN belongs to the same nuclease family
34 as that of the nsp14 coronavirus ExoN ; which has been recently shown to promote viral RNA
35 synthesis proofreading; we propose that Arenavirus ExoN is involved in a “limited RNA editing”
36 mechanism mainly controlled by structural constraints and a low mutational/fitness ratio.

37 **Author summary**

38 Only *Arenaviridae* and *Coronaviridae* encode a 3’-5’ RNA exonuclease domain (ExoN) in
39 their genome. This activity is either used to counteract the innate immunity response during viral
40 infection or to ensure genome stability during replication. Mopeia virus (MOPV), the eastern
41 African counterpart of Lassa virus, carries such ExoN domain, but does not suppress the host innate
42 immunity. We studied MOPV ExoN activity both *in vitro* and *in cellula* to assess the role of ExoN

43 MOPV and found that the Arenaviral ExoN is fully active on dsRNA, and is able like the one of
44 *Coronaviridae* to excise a mismatched base. We measured genetic stability and found evidence of a
45 limited spectrum of RNA synthesis proofreading mechanism, together with a strongly impacted
46 viral replication. We propose that the Arenaviral ExoN is involved in a functional check of the
47 conserved RNA structures of the viral genome.

48 **Introduction**

49

50 *Arenaviridae* is a family of viruses that cause chronic infections of rodents and constitutes a
51 reservoir of human pathogens across the world [1]. Already with a global distribution Lymphocytic
52 choriomeningitis virus (LCMV) is the prototypic member of the family; it is one of the most studied
53 virus and still an underestimated threat to human health [2–6]. In South America, Machupo
54 (MACV), Guanarito, Junin, Sabia, and Chapare viruses are responsible for hemorrhagic fever [7]
55 while in Africa Lujo [8] and Lassa viruses (LASV) constitutes a major public health concern [9–
56 13]. Indeed, LASV is responsible for several hundred thousand infections per year alone [14]. It is a
57 common endemic infection in West Africa (Sierra Leone, Guinea, Liberia, Nigeria) responsible for
58 hearing loss, tremors and encephalitis [13,15]. Moreover, this endemic infection frequently spikes a
59 high number of Lassa fever cases associated with significant mortality and high morbidity. The last
60 episode started in February 2018, in the Niger delta region, presents a case fatality rate around 25 %
61 [16]. This new epidemic reinforces the trends observed during the recent epidemics in Nigeria and
62 Benin in January 2016 [17,18], indicating an increase in virulence, an expansion of spreading areas
63 and the number of cases [19]. Humans become infected through contact with infected rodent
64 excreta, tissues, or blood. Person-to-person transmission of Lassa fever can also occur particularly
65 in the hospital environment in the absence of adequate infection control measures [20]. Until now,
66 no licensed vaccine is available, and therapeutic options are limited to early administration of

67 ribavirin. Despite its public health significance, and recent major contributions [21–25],
68 *Arenaviridae* biology is still poorly understood.

69 *Arenaviridae* are negative-sense single-stranded RNA segmented viruses, with a genome
70 consisting of two segments L (~7.2 kb) and S (~3.4 kb). Each segment has an ambisense coding
71 mechanism, encoding two proteins in opposite orientation, separated by an intergenic region (IGR).
72 The L RNA segment encodes a large protein L (~200 kDa) and a small disordered protein Z (~ 11
73 kDa) [1]. L is a multi-domain protein including in its N-terminus an endonuclease domain followed
74 by a polymerase domain and in its C-terminus a cap binding like domain (for review [26]). Z, which
75 contains a RING finger motif, is a multifunction protein regulating the life cycle of the virus and
76 during budding assembles to form the matrix [27–29]. The S RNA encodes the precursor of mature
77 virion glycoprotein GP-C (75 kDa); that will give after post-translational cleavage GP-1 (40 to 46
78 kDa) and GP-2 (35 kDa) [30,31]; and nucleoprotein NP (~ 63 kDa) [25,32]. NP forms a polymer
79 protecting the genomic (and anti-genomic) RNA (RNA_v) [33]. L and NP together with RNA_v form
80 an active ribonucleic complex (RNP) for replication and transcription [34]. In addition to this
81 critical function, NP is involved in clearing off the cytoplasm of double stranded RNAs (dsRNA),
82 through its C-terminal exonuclease domain (ExoN) [25,32,35–37]. These dsRNAs are markers of
83 viral infection in the cell and are triggering host innate immunity response. Indeed, when dsRNA is
84 detected by proteins such as retinoic acid-inducible I (RIG-I) or melanoma differentiation-
85 associated 5 (MDA- 5), it initiates a signaling pathway that result in the translocation of interferon
86 (IFN) regulatory factor 3 (IRF-3) to the nucleus [38,39]. Then, IRF-3 activates the expression of
87 IFN- α/β , which initiates the antiviral response in the infected cells and primes neighboring cells for
88 a rapid response to viral invasion. From a modular (sequence and structure) perspective, all NP
89 presents a C-terminal ExoN domain (S1 Fig). The South Eastern African counterpart of Lassa Virus
90 is Mopeia virus (MOPV) [40], a non-pathogenic virus. The NP of these two viruses presents a high

91 sequence identity of about 73%, but contrary to Lassa virus, MOPV infection does not result in
92 innate immunity suppression [41,42] leading us to suspect that the domain was not fully functional
93 against dsRNA. Recent studies reported the structure of Mopeia ExoN domain [43] and evidence of
94 an ExoN activity in NP of MOPV, essential for multiplication in antigen-presenting cells [44]. The
95 observed fold conservation and activity raises questions about the biological role of the NP-exo
96 MOPV, and whether it could be conserved for other functional or structural reasons [26]. In the
97 DNA world, ExoNs are mainly involved in mechanisms of genome stability and error correction
98 during or after DNA synthesis. Yet, in viral RNA world, the existence of ExoN is of rare occurrence
99 as only two families of viruses possess a 3'-5' ExoN member of the DEDD super family:
100 *Arenaviridae* and *Coronaviridae* [25,45–47]. The Coronavirus ExoN is part of the nsp14 protein,
101 associated to the main replicative RNA-dependent polymerase nsp12. During RNA synthesis, nsp14
102 belongs to the replication/transcription complex (RTC), excises mismatched bases occurring during
103 processive RNA synthesis, and contributes to overall RNA synthesis fidelity [47–51].

104 Having noted the structural and functional relatedness of *Arenaviridae* ExoN to the
105 *Coronaviridae* ExoN, we engaged into mechanistic studies of the MOPV ExoN. Here, we present a
106 detailed characterization of the activity of NP-exo MOPV including substrate specificity and ion
107 dependency, compared to the ones of LCMV and MACV. We show that the *Arenaviridae* ExoN is
108 active on 3' mismatched dsRNA substrate mimicking a stalled RNA synthesis intermediate, in a
109 remarkable substrate requirement similarity to Coronavirus nsp14. We report, however, that a
110 mutated NP-exo MOPV abrogating the ExoN activity does not lead to an overall higher mutation
111 rate in the surviving viruses, but rather drastically reduces the number of infectious viruses while
112 increasing the release of non-infectious material from infected cells. Interestingly, few nucleotide
113 substitution types appear to be significantly increased in the ExoN(-), establishing that ExoN is
114 active on its own genomic RNA. All together these results confer potentially significant roles to the

115 ExoN domain in the *Arenaviridae* life cycle.

116 **Material and Methods**

117 **Cloning, mutagenesis, protein production and purification**

118 cDNA corresponding to NP ExoN domain of : MOPV (residues 365-570 - P19239), LCMV
119 (residues 357-559 - NP_694852) and MACV (residues 351-563 - P26578) were cloned into the
120 pETG20A expression vector using the Gateway® method (Invitrogen), which adds a cleavable
121 thioredoxin-hexahistidine tag at the N-terminus. The integrity of the DNA construct was verified by
122 DNA sequencing. The sequences of the primers used to sub cloned each domain were:

123 LCMV forward:

124 GGGGACAAGTTTGTACAAAAAAGCAGGCTTAGAAAACCTGTACTTCCAGGGTTTAAGCT
125 ACAGCCAGACAATGCTTTTAAA ,

126 LCMV reverse:

127 GGGGACCACTTTGTACAAGAAAGCTGGGTCTTATTATGTCACATCATTGGGCCTCTA ,

128 MOPV forward:

129 GGGGACAAGTTTGTACAAAAAAGCAGGCTTAGAAAACCTGTACTTCCAGGGTTTAACCT
130 ACTCTCAGACAATGGA,

131 MOPV reverse:

132 GGGGACCACTTTGTACAAGAAAGCTGGGTCTTATTACAGGACAACTCTGGGA

133 MACV forward:

134 GGGGACAAGTTTGTACAAAAAAGCAGGCTTAGAAAACCTGTACTTCCAGGGTCTAAGA
135 CTAGCAAACCTGACTGAAATGCA , and

136 MACV reverse:

137 GGGGACCACTTTGTACAAGAAAGCTGGGTCTTATTATGCAAAGGCTGCCTTGGGTAGA.

138 Plasmids were used to transformed *E.coli* strain C2566 (NEB) protease-deficient and carrying
139 pRARE plasmid (Novagen). Bacteria were grown in LB medium (AthenaES) at 37°C to an
140 OD_{600nm} of 0.5. Expression was induced with 0.5 mM IPTG, and bacteria were grown shaking at
141 210 rpm overnight at 17°C in presence of 100µM of ZnCl₂. Bacteria were pelleted, frozen, and
142 stored at -80°C.

143 The three domains were purified at 4°C. Frozen pellet were melted on ice, resuspended in lysis
144 buffer (20mM HEPES pH7.5, 300 NaCl, 5 mM imidazole, 5% glycerol, 0,1 mg/ml lysozyme and
145 50 µg Dnase), sonicated, and the lysate was cleared by centrifugation at 20,000 rpm for 30 min.
146 Each protein was first purified by metal affinity chromatography using 2ml of His purTM cobalt
147 column (Thermo Scientific). The tag was removed by cleavage with TEV protease followed by
148 purification on a second cobalt affinity chromatography. Proteins were further purified by gel
149 filtration using superdex 75 column (GE Healthcare) in 20 mM HEPES pH 7.5, 300 mM NaCl, 2
150 mM MgCl₂ and 5% glycerol.

151 Mutants were generated for each domain by introducing single point mutations using the Quick
152 change site-directed mutagenesis kit (Stratagene). The primer sequences used for mutagenesis are
153 listed in the supplementary S1 Table. The presence of *ad hoc* mutations and the integrity of the
154 complete coding region of each mutant were confirmed by sequencing. All the mutants were
155 expressed and purified following the established protocol.

156 **RNA labeling and preparation**

157 Synthetic RNAs used in this study were purchased from Dharmacon or Biomers (HPLC
158 grade). They are listed in S2 Table and their predicted structures are shown in S2 Fig. All sens RNA
159 strands were labeled at their 5' end with [γ -³²P] ATP using protein nucleotide kinase (NEB)

160 according to the manufacturer's instructions. For experiments involving overhang mismatched
161 dsRNA, the dsRNAs were generated by annealing an anti-sense RNA strand containing 3'-phosphate
162 modifications with its 5'-radioactively labeled sens RNA strand. The annealing condition was,
163 heating at 70 °C for 10 min and then cooling down to room temperature (with a primer/template
164 ratio of 1.2:1).

165 **Exonuclease activity assay.**

166 Reactions were carried out in a buffer containing 20 mM Tris-Hcl, 5 mM MnCl₂ (unless
167 specified by 5 mM of: MgCl₂, CaCl₂, or ZnCl₂) and 5 mM DTT. Standard reactions contained 0,25
168 μM of protein (NP-exo MOPV or LCMV or MACV or mutants) and 1,25 μM of radiolabeled RNA
169 substrate. After incubated at 37°C, the reactions were quenched at intervals between 0 and 30
170 minutes by the addition of an equal volume of loading buffer (formamide containing 10mM EDTA).
171 The products were heated at 70°C for 5 minutes, rapidly cooled on ice for 3 minutes followed by
172 separation in a 20% poly-acrylamide gel containing 8 M urea and buffered with 0,5X Tris-borate-
173 EDTA. Gels were exposed overnight to a phosphor screen and then visualized with a
174 phosphoimager FLA-3000 (Fuji). Total RNA degradation products were quantified using Image
175 Guage (Fuji), the speed of cleavage determined and graphs plotted using GraphPad PRISM version
176 6.0. Experiments were carried out at least in triplicate and only representative gels are shown.

177 **Thermal shift assay.**

178 A real-time PCR set-up (Bio-rad) was used to monitor the thermal unfolding of the ExoN
179 domain of NP -MOPV, -LCMV or -MACV alone or in the presence of different divalent ions Mn²⁺,
180 Mg²⁺, Ca²⁺ and Zn²⁺. Proteins were equilibrated in a buffer containing 20 mM HEPES pH 7.5, 300
181 mM NaCl, 5% glycerol. All reactions were set up in a final volume of 25 μl in a 96-well plate with

182 total protein concentration of 1,8 mg/ml, 1x SYPRO Orange and incubated with or without 5 mM
183 of metal ions. The PCR plates were sealed with optical sealing tape (Bio-rad) and incubated in the
184 PCR machine for 2 minutes at 20°C followed by 0,2°C increments to a final temperature of 95°C.
185 Thermal denaturation was monitored using SYPRO Orange (Life Technologies) and the fluorescent
186 intensities were measured at 490 nm excitation and 530 nm emission wavelengths. The unfolding of
187 proteins was monitored by following the increase in fluorescence of the probe as it binds to exposed
188 hydrophobic regions of the denatured protein. The T_m was then calculated as the mid-log of the
189 transition phase of the fluorescence curve using the Boltzmann equation. All measurements were
190 performed in triplicates.

191 **Structure and sequence analysis**

192 Structure and sequence comparison of Arenavirus exonuclease with other viral exonuclease.

193 Structure similarities were search with PDBeFold [52] using the MOPV exonuclease
194 domain as a search model (PDB : 5LRP). Corresponding sequences were aligned based on structure
195 comparison using Expresso [53]. Figures were generated with the programs ESPript-ENDscript
196 [54], WebLogo server [55] and UCSF chimera [56].

197 Sequence retrieval of mammarenavirus L and analysis.

198 All annotated complete protein sequences of Mammarenaviruses L protein were
199 downloaded from NCBI. The dataset of 559 sequences was manually curated using Jalview [57] in
200 order to remove Identical, mis-annotated or complete sequences with undefined amino acid (X).
201 The remaining 395 sequences were aligned using MUSCLE [58] constituting the *Mammarenavirus*
202 (MAMV) dataset. From this latter two dataset are being derived the Mopeia virus dataset of 12
203 sequences, and the Lassa Virus dataset of 277 sequences, as being the closest homologue of Mopeia

204 virus with a large number of sequences. Amino acid composition (%) for position in the sequence
205 corresponding to the Mopeia emerging mutant were calculated with Jalview and represented using
206 WebLogo [55] for the three datasets.

207 **Viral infection and genome sequencing.**

208 The MOPV strain AN21366 (JN561684 and JN561685) was used to establish the reverse
209 genetics system for MOPV. The detailed procedures for virus rescue, production, titration and
210 infection of Vero E6 cells are described in [44]. In brief, the recombinant NP-exo WT and mutant
211 (D390A/G393A) MOPV were used to infect Vero E6 cells using a MOI of 0.01. Supernatants were
212 collected four days post infection. Viral production/titration/infection were repeated iteratively for
213 10 times. For viral titration, the presence of the viruses was revealed by immunostaining in infected
214 cells with a polyclonal rabbit antibody that recognizes the MOPV Z protein (Agrobio, France) and a
215 phosphatase alkaline-conjugated polyclonal goat anti-rabbit antibody (Sigma) and 1-Step
216 NBT/BCIP substrate (Thermo Fisher scientific, Waltham, MA). Results are expressed in Focus
217 Forming Unit per mL (FFU/mL). For RNA quantification, viral RNA were extracted from cell
218 culture supernatants (Qiagen, Courtaboeuf, France) and quantification was performed with the
219 EuroBioGreen qPCR Mix Lo-ROX (Eurobio, Les Ulis, France), using an in house developed assay
220 with 5'-CTTTCCCCTGGCGTGTCA-3' and 5'-GAATTTTGAAGGCTGCCTTGA-3' primers.
221 Deep sequencing analysis of viral genomes was performed as described in [44].

222 **Results**

223 **The MOPV NP-exo exhibits a metal-dependent 3'-5' ExoN activity.**

224 The ExoN domain of NP-MOPV (NP-exo MOPV) was incubated with a 5' radiolabeled 22

225 nt RNA hairpin (HP4, S2A Fig) whose 3'-end is base-paired into a double stranded RNA. The
226 reaction was stopped at intervals of 0.1 , 5 and 30 minutes (Fig 1A). In the presence of Mg^{2+} , NP-
227 exo MOPV is able to cleave this stable RNA hairpin ($\Delta G = -14.7$ kcal/mole) predominantly down to
228 a 18-mer product. After removing the 1st 4 nucleotides, degradation stops at the loop region. A
229 similar experiment in the presence of Mn^{2+} allows further degradation into the loop, whereas ExoN
230 is inactive in the presence of either Zn^{2+} or Ca^{2+} . The laddering degradation pattern visualized on the
231 gel, together with radio-label quantification indicate that it acts in the 3'-5' direction (S2B Fig).
232 Visual examination of degradation kinetics shows, a band-product accumulation prior to G
233 nucleotides, indicating that the latter are slower to remove than Cs. We also tested the ExoN activity
234 of the ExoN domain of NP-LCMV (NP-exo LCMV) (Fig 1A) and ExoN domain of NP-MACV
235 (NP-exo MACV) (S3A Fig) on the same RNA substrate. Both proteins cleave the RNA following a
236 similar degradation pattern and comparable kinetics (S2B Fig and S3 Table). All three ExoNs
237 exhibit their highest activity in the presence of Mn^{2+} , followed by Mg^{2+} and they are inactive in the
238 presence of either Ca^{2+} or Zn^{2+} or EDTA (Fig 1A). These results show that the nature of the ions is
239 altering the ExoN activity and its associated pattern of degradation can be greatly modulated by the
240 nature of the metal ion co-factor.

241 **Stabilizing effect by ion cofactor is not correlatable to NP-exo activity.**

242 To study the effect of divalent metal binding on the stability of NP-exo MOPV, we measured
243 the change in melting temperature (T_m) by a Thermal Shift Assay (TSA) in the presence of 5 mM
244 of several metal ions. NP-exo MOPV without metal ions has a T_m of 49.4 °C. Positive T_m shifts
245 are observed in the presence of $MnCl_2$ (+16.5 °C), $MgCl_2$ (+4.9 °C), $CaCl_2$ (+7.5 °C) and a slight
246 negative shift in $ZnCl_2$ (-2.2 °C) (Fig 2). Simultaneously we compared the effect of these ions on
247 the stability of NP-exo LCMV and MACV (Fig 2 & S3B Fig). The T_m values for NP-exo LCMV

248 and NP-exo MACV without metal ions are 50.6 °C and 57.7 °C respectively. For both proteins T_m
249 increases in the presence of MnCl₂ (+13.6°C for LCMV and +7.3 °C for MACV), MgCl₂ (+6 °C
250 for LCMV and +1.7 °C for MACV), CaCl₂ (+7.67 °C for LCMV and +4 °C for MACV) and
251 decreases with ZnCl₂ (-10.3 °C for LCMV and -17.8 °C for MACV). These results indicate that the
252 ion stabilization pattern for each ExoN is unique nevertheless, a similar stabilization trend is
253 observed with MnCl₂ inducing highest stability in all ExoNs. It is also worth noting that CaCl₂
254 which inhibits the 3'-5' ExoN activity is a better stabilizer than MgCl₂.
255 Our results show that stability and activity are uncoupled : lowering the energy of the domain is not
256 key for activation. Rather the nature of the ion plays a key role : the small radius and higher
257 coordination of Mn²⁺ over Mg²⁺ allow a higher number of water molecules available for being
258 activated for the nucleophilic attack. On the contrary, Ca²⁺ with a larger radius slightly deforms the
259 catalytic site [43] and increases the distances with the substrate, thus impairing the reaction.

260 **NP-exo MOPV catalytic residues compared to NP-exo LCMV and MACV.**

261 We mutated each catalytic residue to alanine in order to assess their respective contribution
262 in the conserved DEDDh catalytic motif, and tested them for ExoN activity. For the NP-exo MOPV
263 mutants D390A, E392A and D534A, the 3'-5' ExoN activity is completely abolished whereas
264 D467A and H529A are still able to slowly excise up to two nucleotides. For the NP-exo LCMV
265 mutants, a slightly different result is observed. D382A and E384A show a complete loss of activity,
266 D459A excises two nucleotides but more efficiently than D467A of NP-exo MOPV as judged by the
267 diminution of the 22 nt band-product. The H517A also shows residual activity while the D522A is
268 able to degrade almost the total amount of 22 nt dsRNA up to 20/19 nts (Fig 1A). For NP-exo
269 MACV only the E382A mutant was tested which also shows complete loss of activity (data not
270 shown). We compared the efficacy of cleavage between the wild type NP-exo MOPV and NP-exo

271 LCMV to their corresponding mutants D467A and D459A respectively. Our kinetic experiment
272 indicates that the initial excision rate of NP-exo MOPV and NP-exo LCMV wild types are similar,
273 the rate of D459A of LCMV decreases to about half that of the wild-type, and that of MOPV
274 D467A is significantly affected (S4 Fig).

275 **NP-exo MOPV dsRNA substrate specificity.**

276 In order to investigate the substrate requirement for all three NP-exo MOPV, NP-exo LCMV
277 and NP-exo MACV, we tested their activities on different RNA substrates HP4, A30 (poly A) and
278 LE19. All these single stranded RNA (*ss*RNA) forms several types of secondary structures RNA,
279 which were predicted using Mfold server [59] (S2A Fig). The ExoN assay confirms and extends
280 findings shown in Fig 1, *i.e* that NP-exo MOPV and NP-exo LCMV cleave RNA substrates whose
281 3' ends are engaged into a double stranded structure (Fig 3), consistent with a strict specific double
282 stranded RNA requirement. It is particularly striking in the case of LE19 : at time 0, we observed
283 the 3 species of secondary structures (migration for type A : 19 , B: 18 and C : 17 nucleotides
284 respectively) and with time the top band-product disappears to the profit of an RNA of 17
285 nucleotides. We observed that NP-exo seems to be partly active on small secondary structure *ds*RNA
286 but is inactive on *ss*RNA (Fig 3). NP-exo MACV also shows a similar behavior (S3A Fig).

287

288 As the NP-exo MOPV presents similar *in vitro* behavior to other Arenavirus NP-exo, we
289 conclude that the ExoN activity *per se* is not responsible for immune suppression, and that the latter
290 is mediated by elements embedded in the domain itself. It was thus of interest to better characterize
291 the substrate specificity of the NP-exo in order to disclose its role in arenavirus replication.

292 **NP-exo is able to excise a dsRNA 3'-end mismatch.**

293 We measured NP-exo MOPV and NP-exo LCMV's ability to cleave different dsRNA
294 substrates. Because the key enzyme in the innate immune response; the protein kinase RNA-
295 activated (PKR); is induced by the presence of dsRNA, we made use of a perfectly annealed dsRNA,
296 as well as several potential RNA substrates such as those mimicking an erroneous replication
297 product with one, two or three mismatched nucleotides at the 3'-end. To that end, a 40-mer RNA
298 template (RT1) blocked in 3'-end with a phosphate group was annealed to a radiolabeled RNA
299 carrying zero (RL2*) or one (RL3*), two (RL4*) or three (RL5*) non-complementary nucleotides
300 at its 3'-end as shown in Fig 4A. Fig 4B shows that both enzymes are strict dsRNA ExoNs, with the
301 interesting specific ability to digest substrates carrying a single 3'-terminal mismatch (RL3*/RT1).
302 Quantification of total product (Fig 4C) shows a comparable hydrolytic activity between the
303 perfectly annealed dsRNA and a single 3'-terminal mismatch. The cleavage efficiency, however,
304 drastically drops with the number of unpaired bases at the 3'-end.

305 **The arenavirus NP-exo domain is structurally and functionally similar to the Coronavirus** 306 **RNA 3'-mismatch excising ExoN.**

307 The overall fold of NP-exo MOPV is homologous to that of the other arenavirus ExoNs
308 [43]. Structural comparison reveals that the structure of NP-exo MOPV is very similar to that of
309 LASV, LCMV and Tacaribe virus (TCRV) structures with overall r.m.s.d of ~ 1 Å or less, while the
310 residues of the catalytic site are perfectly superimposed. Indeed, the four conserved catalytic
311 residues (D390 E392 D467 H529 D534) from NP-exo MOPV are located at virtually identical
312 positions as those of the other three ExoNs with only minor differences in their orientations. The Zn
313 coordinating residues (E400, C507, H510 and C530) which are highly conserved in arenaviruses are
314 also oriented in an identical manner in all four structures.

315 A fold similarity search retrieved three ExoN of various origin, namely *Arenaviridae*,

316 *Coronaviridae*, and a human histone mRNA 3'-ExoNs (S5A Fig). Not only the catalytic core of all
317 these enzymes is conserved (S5B Fig), but also they all possess the ability to remove few unpaired
318 nucleotides in the 3'-to-5' direction. We analyzed comparatively the NP-exo MOPV structure and
319 the nsp14 SARS-CoV protein (Fig 5) which also possesses a 3'-exoribonuclease activity able to
320 excise 3'-end mismatch on dsRNA [47]. The comparison of their topology and of their active site
321 shows that secondary structure elements belonging to the catalytic core are arranged in a similar
322 manner. Our results suggest a common origin of the *Coronaviridae* Nsp14 and *Arenaviridae* NP
323 ExoNs.

324 **The arenavirus NP-exo domain affects viral replication but is not involved in genome stability.**

325 To assess the possible role of the NP-exo activity in viral replication and/or genome
326 stability, we passaged iteratively 10 times in Vero E6 cells at a MOI of 0.01 a NP-exo defective
327 virus (NP-exo(-)) carrying the D390A/G393A mutants as well as a NP-exo WT recombinant MOPV.
328 We first quantified both the infectious titers (Fig 6A, left axis) and the NP RNA viral loads (Fig 6A,
329 right axis) of the cell culture supernatants. Our results showed that the infectious viral titers of both
330 viruses followed a parallel trend, the NP-exo(-) always presenting a 40 (minimum, passage 4) to
331 190 (maximum, passage 6) fold decrease in titer compared to the NP-exo WT MOPV. From
332 passages 1 to 5/6, infectious titers continuously decreased (down to a 5 fold for the WT and down a
333 90 fold for the mutant compared to passage 1) before a rebound from passage 6 to 8/9 to titers
334 similar to those of passage 2 followed by another general decrease at passage 10. The viral loads of
335 NP-exo WT and NP-exo(-) MOPV described the same trends as the infectious viral titers albeit with
336 less pronounced variations. The viral load for the WT virus remained stable along the passages with
337 a maximum 3 fold difference while the NP-exo(-) virus had a maximum 13 fold difference.
338 We also calculated the RNA/FFU ratio for both viruses (Fig 6B). On average, the NP-exo WT and

339 NP-exo mutant viruses respectively presented one infectious particle for 3600 and 23000 NP RNA
340 copies, respectively. Interestingly, the maximum ratio was reached at passage 5 for both viruses
341 with 1 FFU for 11300 copies for the WT NP-exo and 1 FFU for 119600 copies for the NP-exo(-).
342 Therefore, the suppression of the NP-exo activity of MOPV promoted both a reduction of the
343 infectious titer and an increased amount of non-infectious material released from infected cells.
344 We next investigated the genomic stability of these two viruses at passage 1 and 10 through deep
345 sequencing analysis. We almost reached a complete coverage of the MOPV genomes except for the
346 5' and 3' end and most of the intergenic region of both segments. The tandem repeated and
347 complementary sequences promote strong secondary structures in the intergenic regions and may
348 explain the lack of reads observed for this region for both viruses.
349 The presence of WT NP sequences detected at passage one for both viruses likely originated from
350 the plasmid expressing the WT NP ORF used for rescuing the virus (data not shown). To make sure
351 our results matched a standard threshold usually observed with the presence of an internal control of
352 sequencing, we considerate a 5% cutoff as a significant read percentage for the effective presence of
353 a mutation (minimum mean coverage of 2636 reads for the L segment of the NP-exo(-) virus and
354 maximum mean coverage of 12610 reads for the S segment of the NP-exo WT virus). As shown in
355 Table 1 & S4, mutations targeting either the ORFs or the UTR/IGR regions are already present in
356 both segments of the NP-exo WT and NP-exo(-) viruses (2.90 and 2.15 mutations/kb respectively)
357 as early as passage one in VeroE6 cells after the virus rescue in BHKT7 cells. The overall mutation
358 rate slightly increases comparatively at passage ten with 3.93 mutations/kb for the NPexo WT virus
359 and 3.36 mutations/kb for the NP-exo(-) virus. Theses results indicate that NP ExoNs does not
360 affect the overall genome stability but affects the viral replication.

361

362 **The arenavirus NP-exo domain is active on its own genome.**

363 We observe that the overall mutation rate is stable between NP-exo WT and NP-exo(-) MOPV, yet
364 we also notice that the frequency of these mutations has changed. We observe at passage 10 a
365 comparable number of mutations along the S segment but a decrease of ~ 22 % on the L segment of
366 the mutant together with an increase of their occurrence frequencies. For both, these mutations
367 appears along the entire L segment at an average frequency of ~ 10.1 % (comprised between 5 to 24
368 %) for the WT and of ~ 16.6 % (comprised between 5 to 93 %) for the mutant, in particular the
369 substitution of C to T. While for the S segment mutations appear along the entire for the WT and
370 clustered for the mutant at respective frequencies of 14.6 % and 19.5 %.

371 Among all mutations recorded, only a few were present for either both viruses and/or at the two
372 different passages. Indeed, three mutations in the S segment and one mutation in the L segment are
373 present for both viruses at passages one and ten and likely represent stable quasi-species (Table S4,
374 and Table 1 yellow highlight).

375 Three mutations in the L segment are commonly found for the two viruses only at passage 10 (Table
376 1, orange highlight). Interestingly, three non-synonymous mutations in the L-polymerase ORF
377 (S184L, S1021P and L1477S, Table 1, red highlight) became majority for the NP-exo(-) virus at
378 passage 10.

379 To ascertain the trend observed in our genomic sequencing data, we investigated the natural
380 occurrence of these mutations in *Mammarenavirus* (MAMV) using bioinformatics. The pre-
381 supposed being that if these mutations appear randomly they should be significantly (> 5 %)
382 represented in the general population of MAMV and LASV.

383 From the three subsets of sequences generated; *i.e* MAMV, LASV and MOPV; we observed that the
384 three mutations S184L, S1021P and L1477S appeared in conserved regions in all three subsets, that
385 none of the three mutants were reported in MOPV subset and finally that the three amino acid are

386 subject to diverse selective pressure (Fig 7). Indeed, serine at the position 184 represents the
387 majority of the observed amino acid variants while the specific mutation S184L represents only 1 %
388 of the total observed sequences in the LASV or MAMV subsets. This observation indicates that the
389 mutation is viable but most likely costly to be maintained by the virus. On the other hand, at
390 position 1021, the serine observed in MOPV subset does not represent the majority of the observed
391 amino acid in the other subsets, the proline is by far the most frequent amino acids found (Fig 7). In
392 LASV, the serine subset represents only 3% of the observed amino acids at this position while 10%
393 in the MAMV subset (Fig 7). This observation indicates that this position in MOPV is an oddity
394 compared to the others. It seems that the natural tendency in the L protein is to have a proline rather
395 than a serine at this position. The fact that we observe that particular reversion in the NP-Exo(-)
396 could indicate that for L MOPV there is a constraint at this particular position. Finally, at position
397 1477, the amino acid found at this position for the three subsets is a leucine (Fig 7), indicating that,
398 that particular position is under a high selective pressure. The mutation L1477S was never observed
399 in any subsets, this mutation can be interpreted as unlikely and therefore considered as direct
400 consequence of the NP-Exo(-).

401 Our results show that compared to the WT virus, the abrogation of the NP-exo activity did not
402 increase the mutation rate found in the MOPV genomic sequences present in the cell culture
403 supernatant, but the emergence of the three mutants of rare occurrence are the direct consequence of
404 the NP-Exo(-), which have relaxed the control over certain position implying a direct effect of the
405 MOPV exonuclease on its own genomic RNA.

406

407 **Discussion**

408 The paradigm of *Arenaviridae* NP ExoN states that it is involved in innate immunity
409 suppression [37,60–62], through degradation of dsRNAs which would otherwise stimulate the innate

410 immunity response. Several reports have demonstrated that NP is responsible for the degradation of
411 these dsRNAs using the 3'-5' ExoN located at its C-terminus [25,32,35,63]. This ExoN comprises a
412 DEDDh catalytic motif that is completely conserved across the *Arenaviridae* [35] implying this
413 activity may be a general feature of arenavirus NPs. The ExoN domain is conserved within the
414 family regardless of both the virus pathogenic potential and its ability to suppress efficiently type I
415 IFN, as previously reported for TCRV and MOPV [42,60,64]. MOPV is the closest counterpart of
416 LASV and presents a 73% NP sequence identity with LASV. During LASV infections, the virus
417 targets mainly macrophages (MP) and dendritic (DC) cells [65], and infections are characterized by
418 high viremia and generalized immune suppression supposedly due to innate immune inhibition by
419 the ExoN domain. Both MOPV and LASV induces strong type I IFN responses in MP and
420 moderately in DC, but contrarily to LASV which abrogates this response, MOPV does not [42,64].

421 Our functional study demonstrates that the ExoN structure, substrate specificity, and
422 mechanism is indeed conserved across the family. It is also clear from the structure-ion analysis
423 [43], that toying with the catalytic ion leads to slight structural changes which impact dramatically
424 the activity. Although NP-exo MOPV, NP-exo LCMV have similar cleavage patterns, mutation
425 analysis of the DEDDh motif reveals that the exact residues critical for 3'-5' ExoN vary between
426 both domains. For NP-exo MOPV, D390A, E392A and D534A (D389A, E391A and D533A LASV
427 equivalents) completely abolishes 3'-5' ExoN activity consistent with results from *in vitro* studies on
428 LASV [35], while D467A and H529A (D466A and H529A LASV equivalents) retains some
429 residual activity (see below). For NP-exo LCMV, a previous study by Martínez-Sobrido and
430 collaborators [61], correlated innate immunity suppression to ExoN mutants, postulating a direct
431 involvement of the ExoN activity. We observed that mutant D382A completely loses ExoN activity
432 consistently with results from reverse genetic studies [61]. A noticeable difference concern the
433 mutant E384A, that was shown to have no effect and be dispensable for ExoN activity [61], is

434 rather shown critical in our *in vitro* study and consistent with the structural data as E384 (equivalent
435 to MOPV E392) is involved in binding one of the catalytic ion (S6 Fig). Under our conditions,
436 D459A and H517A still retains their ability to cleave two nucleotides meanwhile D522A shows a
437 significant activity leading to the removal of two to three nucleotides. These latter three mutants
438 were not reported before but the analysis of the structure of NP-exo MOPV confirms that major
439 features such as fold, and the two ion binding sites (catalytic and structural) are conserved within
440 the *Arenaviridae* [25,32,35,36,63]. Residues D390, E392, D534 of NP-exo MOPV directly
441 coordinate the catalytic ion. Mutation of these residues logically alter ion binding and thus leads to
442 complete loss of catalytic activity. The residual activity observed for D522A of NP-exo LCMV is
443 rather difficult to explain as the two structures present no clear differences in the ion binding mode.
444 The only noticeable difference is about the hydrophobic environment that may compensate the
445 faulty metal-binding site in the case of NP-exo LCMV. The residual activity observed for D467
446 (D459 of LCMV) is rather difficult to explain as the two structures present no clear differences, yet
447 that residue is very likely involved in the cleavage mechanism. Indeed, the kinetic experiments
448 comparing the WT NP-exo MOPV and NP-exo LCMV to corresponding mutants show that the first
449 event of the hydrolysis is comparable between NP-exo MOPV and NP-exo LCMV, while mutation
450 of the aspartate reduces drastically the hydrolysis kinetics for NP-exo MOPV but only moderately
451 for NP-exo LCMV (S4 Fig). These differences suggest that the aspartate (respectively D467, D459)
452 is involved in the structural set-up of the active site for positioning the ion responsible for the
453 nucleophilic attack. The general mechanism for RNA hydrolysis is a two metal ion mechanism
454 described by Steitz and Steitz [66]. It involves metal A and B positioned ~ 4 Å apart each other and
455 across the target phosphodiester bond. Metal ion A facilitates the formation of the attacking
456 nucleophile. This is followed by the formation of a penta-covalent intermediate which is stabilized
457 by both metal ions. Metal ion B then eases the exit of the leaving group. With the help of the LASV

458 structures of Jiang and collaborator [36], we made an attempt to reconstitute a model of the general
459 mechanism for RNA hydrolysis (S6A Fig). In NP-exo MOPV structure (and all the others) only the
460 metal B is visible. The site receiving the other catalytic metal A is partly created with interaction of
461 the RNA and residues D390 and D467 (S6B Fig). The interaction between the ion in position A and
462 D467 is mediated through a water molecule. Therefore, this might explain why this mutant retained
463 a partial residual activity.

464 As it was shown for TCRV, the ExoN domain of MOPV *in vitro* is endowed with full ExoN
465 activity and obeys to the same structural and energetic constraints as those of other *Arenaviridae*
466 ExoNs [36,43]. Therefore MOPV ExoN activity alone is not *per se* responsible for the differences
467 in innate immunity suppression between MOPV and LASV. Rather, the presence of the ExoN
468 activity may serve other purposes in the viral life cycle, which might be connected directly or
469 indirectly to innate immunity.

470 In particular, previous studies on LCMV and PICV suggested that altering the NP ExoN also
471 impacts replication, irrespective to the IFN status of the host cell [61,67]. The structural relatedness
472 with the Coronavirus ExoN and its implication in viral replication prompted us to investigate to
473 which extent the arenavirus ExoN domain is able to excise unpaired nucleotides. Our enzyme
474 activity assays demonstrate that NP-exo MOPV and NP-exo LCMV can efficiently and selectively
475 cleave a dsRNA mimicking an erroneous replication product carrying one 3'-mismatched nucleotide
476 (Fig 4). Our analysis confirms that despite additional inserted structural elements, the two domains
477 belong to the same Ribonuclease H-like superfamily. In the case of *Coronaviridae*, several studies
478 have pointed to a main role of the ExoN domain of nsp14 in RNA proofreading [47–50] to maintain
479 genome stability. Structural comparison between ExoN domain of nsp14 and MOPV shows
480 conservation of active site and main fold (Fig 5) suggesting that they have a distant but common
481 origin. Recent work by Becares and colleagues have shown that nsp14 of Coronavirus is also

482 involved in innate immunity modulation [68]. Therefore, these data show that at least in
483 *Coronaviridae* the 3'-5' ExoN activity is not exclusively assigned to a specific role but is involved in
484 different aspect of the viral life cycle. Our study present clear evidence that much like the
485 coronavirus nsp14 [47], the *Arenaviridae* NP ExoN excises a 3'-end mismatch dsRNA *in vitro*, and
486 based on previous report that this activity is directly connected to RNA replication [61,67].

487 From our data, the MOPV polymerase exhibits an average error rate estimated around 3
488 mutations / kb. This means that the polymerase was able to incorporate a mismatch and then
489 elongate it. The error rate does not change between the WT and the mutant, which is consistent with
490 the fact that we did not altered the polymerase. For both, these mutations appears along the entire L
491 segment at an average frequency of ~10.1 % (comprised between 5 to 24 %) for the WT and of
492 ~16.6 % (comprised between 5 to 93 %) for the mutant. The fact that unlikely mutants have become
493 prevalent, as observed at passage 10, reflect that the control over certain type of mutation have been
494 abolished, thus implicating that ExoN is active on its own genomic RNA. In this study, it is not the
495 particular set of mutations that is relevant but rather that a set of unlikely mutations have emerged.
496 The bias inferred by impairment of the ExoN, together with the biochemistry presented here is
497 consistent with the idea that ExoN is involved in a mismatch excision system.

498 Although the presence of mismatch excision system is logically associated to very large
499 genomes (~30 kb) in *Coronaviridae*, the presence of such activity, and potentially such RNA repair
500 system, in *Arenaviridae* of intermediate genome size (~11 kb) remains puzzling. Our results shows
501 a clear diminution of the viral titer for viruses depleted of ExoN activity, but no clear evidence of a
502 drastic increase of mutation in the genome that would lead to catastrophic event. Then what is
503 happening in these mutated viruses? One tentative explanation could be the ExoN is involved in : i)
504 checking and maintaining the sequence integrity of the conserved genomic region at its extremities,
505 and/or ii) the structural integrity of the Intergenic Region (IGR). Indeed, both regions have been

506 previously reported as being critical for viral fitness: *i*) The conserved region (19 nucleotides)
507 exhibit high degree of sequence conservation at the 3'-termini and is complementary to the 5' end of
508 the genome (for review [26]). This sequence serves as a selective docking platform for the
509 polymerase [69] for which 3'-end binds with high affinity and in a sequence specific manner [70].
510 *ii*) Similarly, alteration of the IGR structure leads to reduce efficient transcription termination and
511 viral assembly [71,72]. In such hypothesis, the impairment of the NP-exo activity leads to a
512 scenario in which the polymerase is able to incorporate a mismatch but is unable to elongate it,
513 leading to a decrease of suitable genomic material to package, therefore without the ExoN control
514 the number of functional RNP would be reduced and consistent with the loss of viral fitness
515 observed here and else [61,67]. Therefore we propose that the Arenavirus ExoN is involved in a
516 “limited proof-reading” mechanism driven by structural constraints rather than genomic stability.
517 Another observation that concurs to the “limited proof-reading” mechanism is the difference of
518 Ribavirin efficiency on *Arenaviridae* and *Coronaviridae*. Ribavirin is the only drug so far
519 administered on large scale and having demonstrated a decrease of mortality rates up to 5%, if
520 administered within the first 6 days of arenaviral illness [73]. On the other hand, Ribavirin is
521 ineffective against coronaviruses [74,75], as nsp14 ExoN domain excises the nucleotide analogue
522 [51]. It is likely, that for *Arenaviridae*, the ExoN activity involved in a “limited proof-reading”
523 mechanism remains as a trace of its past common ancestor with *Coronaviridae*. The critical
524 problem of genomic stability being solved, either by the conservation of the “original” function of
525 the ExoN for *Coronaviridae*, or by genome segmentation for *Arenaviridae*.

526

527 As a conclusion we have shown that the MOPV ExoN is fully functional, behaving like
528 other Arenaviral ExoN on dsRNA. We have demonstrated that Arenaviral ExoN are able to excise an
529 RNA mismatch, and that is active on its own genomic RNA like its counterpart in *Coronaviridae*.

530 Under the conditions used here, abrogation of ExoN activity does not impact genomic stability
531 significantly. Our results suggest that the *Arenaviridae* RNA ExoN, like that of *Coronaviridae*, is at
532 a crossroad between replication efficiency and innate immunity evasion in the infected cell.

533

534 **Acknowledgments**

535 This work was supported by ANR grants ArenaBunya-L (ANR-11-BSV8-0019), the Centre
536 National de la Recherche Scientifique (CNRS), the Fondation Infection Méditerranée, and the
537 French Infrastructure for Integrated Structural Biology (FRISBI) ANR-10-INSB-05-01. The authors
538 also thank Dr. Barbara Selisko for her help and useful discussion and Julie Lichère for her
539 contribution in the experiments.

540

541 **References**

1. Buchmeier MJ, de la Torre J-C, Peters CJ, Torre JD. Arenaviridae: The Viruses and Their Replication. In: Knipe DM, Howley PM, editors. *Fields Virology*. 5th ed. Philadelphia, PA, USA: Lippincott Williams & Wilkins; 2007. pp. 1791–1827.
2. Mets MB, Barton LL, Khan AS, Ksiazek TG. Lymphocytic choriomeningitis virus: An underdiagnosed cause of congenital chorioretinitis. *Am J Ophthalmol*. 2000;130: 209–215. doi:10.1016/S0002-9394(00)00570-5
3. Brézin AP, Thulliez P, Cisneros B, Mets MB, Saron MF. Lymphocytic choriomeningitis virus chorioretinitis mimicking ocular toxoplasmosis in two otherwise normal children. *Am J Ophthalmol*. 2000;130: 245–247. doi:10.1016/S0002-9394(00)00563-8
4. Barton LL, Mets MB, Beauchamp CL. Lymphocytic choriomeningitis virus: Emerging fetal teratogen. *Am J Obstet Gynecol*. 2002;187: 1715–1716. doi:10.1067/mob.2002.126297
5. Barton LL, Peters CJ, Ksiazek TG. Lymphocytic choriomeningitis virus: an unrecognized teratogenic pathogen. *Emerg Infect Dis*. 1995;1: 152–153.
6. Jamieson DJ, Kourtis AP, Bell M, Rasmussen SA. Lymphocytic choriomeningitis virus: An emerging obstetric pathogen? *Am J Obstet Gynecol*. 2006;194: 1532–1536. doi:10.1016/j.ajog.2005.11.040
7. Bowen MD, Peters CJ, Nichol ST. The phylogeny of New World (Tacaribe complex) arenaviruses. *Virology*. 1996;219: 285–290. doi:10.1006/viro.1996.0248
8. Briese T, Paweska JT, McMullan LK, Hutchison SK, Street C, Palacios G, et al. Genetic detection and characterization of Lujo virus, a new hemorrhagic fever-associated arenavirus

from southern Africa. Buchmeier MJ, editor. PLoS Pathog. 2009;5: e1000455–e1000455.

doi:10.1371/journal.ppat.1000455

9. Peterson a T, Moses LM, Bausch DG. Mapping transmission risk of lassa Fever in west Africa: the importance of quality control, sampling bias, and error weighting. PloS One. 2014;9: e100711–e100711. doi:10.1371/journal.pone.0100711
10. Leparc-Goffart I, Emonet SF. [An update on Lassa virus]. Médecine Trop Rev Corps Santé Colon. 2011;71: 541–5.
11. Yun NE, Walker DH. Pathogenesis of Lassa Fever. Viruses. 2012;4: 2031–2048. doi:10.3390/v4102031
12. Mofolorunsho KC. Outbreak of lassa fever in Nigeria: measures for prevention and control. Pan Afr Med J. 2016;8688: 2–4. doi:10.11604/pamj.2016.23.210.8923
13. Günther S, Lenz O. Lassa Virus. Crit Rev Clin Lab Sci. 2004;41: 339–390. doi:10.1080/10408360490497456
14. Centers for Disease Control and Prevention. CDC twenty four Centers for Disease Control and Prevention. Lassa Fever [Internet]. Available: <https://www.cdc.gov/vhf/lassa/>
15. Yun NE, Ronca S, Tamura A, Koma T, Seregin A V., Dineley KT, et al. Animal Model of Sensorineural Hearing Loss Associated with Lassa Virus Infection. Ross SR, editor. J Virol. 2015;90: 2920–7. doi:10.1128/JVI.02948-15
16. WHO Africa. WHO moves to contain Nigeria’s Lassa fever outbreak. In: Disease Outbreak News [Internet]. 2018 [cited 13 Mar 2018]. Available: <http://www.afro.who.int/news/who-moves-contain-nigerias-lassa-fever-outbreak>

17. W.H.O. Lassa Fever – Nigeria. In: Disease Outbreak News [Internet]. 2016 [cited 8 Aug 2016]. Available: <http://who.int/csr/don/27-may-2016-lassa-fever-nigeria/en/>
18. W.H.O. Lassa Fever – Benin. In: Disease Outbreak News [Internet]. 2016 [cited 8 Aug 2016]. Available: <http://www.who.int/csr/don/13-june-2016-lassa-fever-benin/en/>
19. Clegg JC. Influence of climate change on the incidence and impact of arenavirus diseases: A speculative assessment. *Clin Microbiol Infect.* 2009;15: 504–509. doi:10.1111/j.1469-0691.2009.02847.x
20. Fisher-Hoch SP, Tomori O, Nasidi a, Perez-Oronoz GI, Fakile Y, Hutwagner L, et al. Review of cases of nosocomial Lassa fever in Nigeria: the high price of poor medical practice. *BMJ.* 1995;311: 857–9.
21. Sullivan BM, Teijaro JR, de la Torre JC, Oldstone MBA. Early Virus-Host Interactions Dictate the Course of a Persistent Infection. Feng P, editor. *PLoS Pathog.* 2015;11: e1004588–e1004588. doi:10.1371/journal.ppat.1004588
22. Huang C, Kolokoltsova OA, Yun NE, Seregin AV, Ronca S, Koma T, et al. Highly Pathogenic New World and Old World Human Arenaviruses Induce Distinct Interferon Responses in Human Cells. *J Virol.* 2015;89: 7079–88. doi:10.1128/JVI.00526-15
23. Wilson EB, Yamada DH, Elsaesser H, Herskovitz J, Deng J, Cheng G, et al. Blockade of Chronic Type I Interferon Signaling to Control Persistent LCMV Infection. *Science.* 2013;340: 202–207. doi:10.1126/science.1235208
24. Teijaro JR, Ng C, Lee AM, Sullivan BM, Sheehan KCF, Welch M, et al. Persistent LCMV infection is controlled by blockade of type I interferon signaling. *Science.* 2013;340: 207–11.

doi:10.1126/science.1235214

25. Qi X, Lan S, Wang W, Schelde LM, Dong H, Wallat GD, et al. Cap binding and immune evasion revealed by Lassa nucleoprotein structure. *Nature*. 2010;468: 779–783.
doi:10.1038/nature09605
26. Ferron F, Weber F, de la Torre JC, Reguera J. Transcription and replication mechanisms of Bunyaviridae and Arenaviridae L proteins. *Virus Res*. 2017; 1–17.
doi:10.1016/j.virusres.2017.01.018
27. Cornu TI, de la Torre JC. RING finger Z protein of lymphocytic choriomeningitis virus (LCMV) inhibits transcription and RNA replication of an LCMV S-segment minigenome. *J Virol*. 2001;75: 9415–26. doi:10.1128/JVI.75.19.9415-9426.2001
28. Perez M, Greenwald DL, de la Torre JC. Myristoylation of the RING finger Z protein is essential for arenavirus budding. *J Virol*. 2004;78: 11443–11448.
29. Hastie KM, Zandonatti M, Liu T, Li S, Woods VL, Sapphire EO. Crystal Structure of the Oligomeric Form of Lassa Virus Matrix Protein Z. *J Virol*. 2016;90: 4556–62.
doi:10.1128/JVI.02896-15
30. Burri DJ, da Palma JR, Kunz S, Pasquato A. Envelope glycoprotein of arenaviruses. *Viruses*. 2012;4: 2162–81. doi:10.3390/v4102162
31. Hastie KM, Igonet S, Sullivan BM, Legrand P, Zandonatti MA, Robinson JE, et al. Crystal structure of the prefusion surface glycoprotein of the prototypic arenavirus LCMV. *Nat Struct Mol Biol*. 2016;23: 513–521. doi:10.1038/nsmb.3210
32. Brunotte L, Kerber R, Shang W, Hauer F, Hass M, Gabriel M, et al. Structure of the Lassa

- virus nucleoprotein revealed by X-ray crystallography, small-angle X-ray scattering, and electron microscopy. *J Biol Chem*. 2011;286: 38748–56. doi:10.1074/jbc.M111.278838
33. Hastie KM, Liu T, Li S, King LB, Ngo N, Zandonatti M a, et al. Crystal structure of the Lassa virus nucleoprotein-RNA complex reveals a gating mechanism for RNA binding. *Proc Natl Acad Sci U S A*. 2011;108: 19365–70. doi:10.1073/pnas.1108515108
34. Pinschewer DD, Perez M, de la Torre JC. Role of the virus nucleoprotein in the regulation of lymphocytic choriomeningitis virus transcription and RNA replication. *J Virol*. 2003;77: 3882–3887.
35. Hastie KM, Kimberlin CR, Zandonatti MA, MacRae IJ, Saphire EO. Structure of the Lassa virus nucleoprotein reveals a dsRNA-specific 3' to 5' exonuclease activity essential for immune suppression. *Proc Natl Acad Sci U S A*. 2011;108: 2396–401. doi:10.1073/pnas.1016404108
36. Jiang X, Huang Q, Wang W, Dong H, Ly H, Liang Y, et al. Structures of arenaviral nucleoproteins with triphosphate dsRNA reveal a unique mechanism of immune suppression. *J Biol Chem*. 2013;288: 16949–59. doi:10.1074/jbc.M112.420521
37. Ortiz-Riaño E, Cheng BYH, de la Torre JC, Martínez-Sobrido L. The C-Terminal Region of Lymphocytic Choriomeningitis Virus Nucleoprotein Contains Distinct and Segregable Functional Domains Involved in NP-Z Interaction and Counteraction of the Type I Interferon Response. *J Virol*. 2011;85: 13038–48. doi:10.1128/JVI.05834-11
38. Yoneyama M, Onomoto K, Fujita T. Cytoplasmic recognition of RNA. *Adv Drug Deliv Rev*. 2008;60: 841–6. doi:10.1016/j.addr.2007.12.001

39. Yoneyama M, Kikuchi M, Natsukawa T, Shinobu N, Imaizumi T, Miyagishi M, et al. The RNA helicase RIG-I has an essential function in double-stranded RNA-induced innate antiviral responses. *Nat Immunol.* 2004;5: 730–7. doi:10.1038/ni1087
40. Bowen MD, Rollin PE, Ksiazek TG, Hustad HL, Bausch DG, Demby AH, et al. Genetic Diversity among Lassa Virus Strains. *J Virol.* 2000;74: 6992–7004. doi:10.1128/JVI.74.15.6992-7004.2000
41. Lukashevich IS, Maryankova R, Vladyko a S, Nashkevich N, Koleda S, Djavani M, et al. Lassa and Mopeia virus replication in human monocytes/macrophages and in endothelial cells: different effects on IL-8 and TNF-alpha gene expression. *J Med Virol.* 1999;59: 552–560. doi:10.1002/(SICI)1096-9071(199912)59:4<552::AID-JMV21>3.0.CO;2-A
42. Pannetier D, Faure C, Georges-Courbot M-C, Deubel V, Baize S. Human macrophages, but not dendritic cells, are activated and produce alpha/beta interferons in response to Mopeia virus infection. *J Virol.* 2004;78: 10516–24. doi:10.1128/JVI.78.19.10516-10524.2004
43. Yekwa E, Khourieh J, Canard B, Papageorgiou N, Ferron F. Activity inhibition and crystal polymorphism induced by active-site metal swapping. *Acta Crystallogr Sect Struct Biol.* 2017;73: 641–649. doi:10.1107/S205979831700866X
44. Carnec X, Mateo M, Page A, Reynard S, Hortion J, Picard C, et al. A Vaccine Platform against Arenaviruses Based on a Recombinant Hyperattenuated Mopeia Virus Expressing Heterologous Glycoproteins. *J Virol.* 2018;92: 1–17. doi:10.1128/JVI.02230-17
45. Eckerle LD, Lu X, Sperry SM, Choi L, Denison MR. High fidelity of murine hepatitis virus replication is decreased in nsp14 exoribonuclease mutants. *J Virol.* 2007;81: 12135–44. doi:10.1128/JVI.01296-07

46. Minskaia E, Hertzog T, Gorbalenya AE, Campanacci V, Cambillau C, Canard B, et al. Discovery of an RNA virus 3'->5' exoribonuclease that is critically involved in coronavirus RNA synthesis. *Proc Natl Acad Sci U S A*. 2006;103: 5108–13. doi:10.1073/pnas.0508200103
47. Bouvet M, Imbert I, Subissi L, Gluais L, Canard B, Decroly E. RNA 3'-end mismatch excision by the severe acute respiratory syndrome coronavirus nonstructural protein nsp10/nsp14 exoribonuclease complex. *Proc Natl Acad Sci U S A*. 2012;109: 9372–7. doi:10.1073/pnas.1201130109
48. Eckerle LD, Becker MM, Halpin RA, Li K, Venter E, Lu X, et al. Infidelity of SARS-CoV Nsp14-exonuclease mutant virus replication is revealed by complete genome sequencing. Emerman M, editor. *PLoS Pathog*. 2010;6: e1000896–e1000896. doi:10.1371/journal.ppat.1000896
49. Denison MR, Graham RL, Donaldson EF, Eckerle LD, Baric RS. Coronaviruses: An RNA proofreading machine regulates replication fidelity and diversity. *RNA Biol*. 2011;8: 270–279. doi:10.4161/rna.8.2.15013
50. Subissi L, Imbert I, Ferron F, Collet A, Coutard B, Decroly E, et al. SARS-CoV ORF1b-encoded nonstructural proteins 12-16: Replicative enzymes as antiviral targets. *Antiviral Res*. 2014;101: 122–30. doi:10.1016/j.antiviral.2013.11.006
51. Ferron F, Subissi L, Silveira De Moraes AT, Le NTT, Sevajol M, Gluais L, et al. Structural and molecular basis of mismatch correction and ribavirin excision from coronavirus RNA. *Proc Natl Acad Sci U S A*. 2018;115: E162–E171. doi:10.1073/pnas.1718806115
52. Krissinel E, Henrick K. Secondary-structure matching (SSM), a new tool for fast protein structure alignment in three dimensions. *Acta Crystallogr D Biol Crystallogr*. 2004;60: 2256–

2268. doi:10.1107/S0907444904026460

53. Armougom F, Moretti S, Poirot O, Audic S, Dumas P, Schaeli B, et al. Espresso: Automatic incorporation of structural information in multiple sequence alignments using 3D-Coffee. *Nucleic Acids Res.* 2006;34: 604–608. doi:10.1093/nar/gkl092
54. Gouet P, Robert X, Courcelle E. ESPript/ENDscript: Extracting and rendering sequence and 3D information from atomic structures of proteins. *Nucleic Acids Res.* 2003;31: 3320–3. doi:10.1093/nar/gkg556
55. Crooks G, Hon G, Chandonia J, Brenner S. WebLogo: a sequence logo generator. *Genome Res.* 2004;14: 1188–1190. doi:10.1101/gr.849004.1
56. Pettersen EF, Goddard TD, Huang CC, Couch GS, Greenblatt DM, Meng EC, et al. UCSF Chimera - A visualization system for exploratory research and analysis. *J Comput Chem.* 2004;25: 1605–1612. doi:10.1002/jcc.20084
57. Brandt BW, Feenstra KA, Heringa J. Multi-Harmony: detecting functional specificity from sequence alignment. *Nucleic Acids Res.* 2010;38: W35-40. doi:10.1093/nar/gkq415
58. Edgar RC. MUSCLE: multiple sequence alignment with high accuracy and high throughput. *Nucleic Acids Res.* 2004;32: 1792–7. doi:10.1093/nar/gkh340
59. Zuker M. Mfold web server for nucleic acid folding and hybridization prediction. *Nucleic Acids Res.* 2003;31: 3406–15.
60. Martínez-Sobrido L, Giannakas P, Cubitt B, García-Sastre A, de la Torre JC. Differential inhibition of type I interferon induction by arenavirus nucleoproteins. *J Virol.* 2007;81: 12696–703. doi:10.1128/JVI.00882-07

61. Martínez-Sobrido L, Emonet S, Giannakas P, Cubitt B, García-Sastre A, de la Torre JC. Identification of amino acid residues critical for the anti-interferon activity of the nucleoprotein of the prototypic arenavirus lymphocytic choriomeningitis virus. *J Virol.* 2009;83: 11330–11340. doi:10.1128/JVI.00763-09
62. Reynard S, Russier M, Fizet A, Carnec X, Baize S. Exonuclease domain of the Lassa virus nucleoprotein is critical to avoid RIG-I signaling and to inhibit the innate immune response. *J Virol.* 2014;88: 13923–7. doi:10.1128/JVI.01923-14
63. Hastie KM, King LB, Zandonatti MA, Sapphire EO. Structural basis for the dsRNA specificity of the Lassa virus NP exonuclease. *PloS One.* 2012;7: e44211. doi:10.1371/journal.pone.0044211
64. Pannetier D, Reynard S, Russier M, Journeaux A, Tordo N, Deubel V, et al. Human dendritic cells infected with the nonpathogenic Mopeia virus induce stronger T-cell responses than those infected with Lassa virus. *J Virol.* 2011;85: 8293–306. doi:10.1128/JVI.02120-10
65. Baize S, Kaplon J, Faure C, Pannetier D, Georges-Courbot M-C, Deubel V. Lassa virus infection of human dendritic cells and macrophages is productive but fails to activate cells. *J Immunol Baltim Md 1950.* 2004;172: 2861–9.
66. Steitz T a, Steitz J a. A general two-metal-ion mechanism for catalytic RNA. *Proc Natl Acad Sci U S A.* 1993;90: 6498–6502. doi:10.1073/pnas.90.14.6498
67. Huang Q, Shao J, Lan S, Zhou Y, Xing J, Dong C, et al. In Vitro and In Vivo Characterizations of Pichinde Viral Nucleoprotein Exoribonuclease Functions. *J Virol.* 2015;89: 6595–6607. doi:10.1128/JVI.00009-15

68. Becares M, Pascual-Iglesias A, Nogales A, Sola I, Enjuanes L, Zuñiga S. Mutagenesis of Coronavirus nsp14 Reveals Its Potential Role in Modulation of the Innate Immune Response. *J Virol.* 2016;90: 5399–414. doi:10.1128/JVI.03259-15
69. Gerlach P, Malet H, Cusack S, Reguera J. Structural insights into bunyavirus replication and its regulation by the vRNA promoter. *Cell.* 2015;161: 1267–1279. doi:10.1016/j.cell.2015.05.006
70. Kranzusch PJ, Schenk AD, Rahmeh AA, Radoshitzky SR, Bavari S, Walz T, et al. Assembly of a functional Machupo virus polymerase complex. *Proc Natl Acad Sci U S A.* 2010; 1–6. doi:10.1073/pnas.1007152107
71. Pinschewer DD, Perez M, de la Torre JC. Dual role of the lymphocytic choriomeningitis virus intergenic region in transcription termination and virus propagation. *J Virol.* 2005;79: 4519–26. doi:10.1128/JVI.79.7.4519-4526.2005
72. Iwasaki M, Cubitt B, Sullivan BM, de la Torre JC. The High Degree of Sequence Plasticity of the Arenavirus Noncoding Intergenic Region (IGR) Enables the Use of a Nonviral Universal Synthetic IGR To Attenuate Arenaviruses. *J Virol.* 2016;90: 3187–97. doi:10.1128/JVI.03145-15
73. McCormick JB, King IJ, Webb PA, Scribner CL, Craven RB, Johnson KM, et al. Lassa fever. Effective therapy with ribavirin. *N Engl J Med.* 1986;314: 20–6. doi:10.1056/NEJM198601023140104
74. Stockman LJ, Bellamy R, Garner P. SARS: Systematic Review of Treatment Effects. Low D, editor. *PLoS Med.* 2006;3: e343–e343. doi:10.1371/journal.pmed.0030343

75. Al-Tawfiq JA, Memish ZA. Update on therapeutic options for Middle East Respiratory Syndrome Coronavirus (MERS-CoV). *Expert Rev Anti Infect Ther.* 2017;15: 269–275.
doi:10.1080/14787210.2017.1271712

543

544 **Figure legends**

545 **Fig 1. Comparison of the ExoN activity of NP-exo MOPV and NP-exo LCMV.** (A) Effect of
546 divalent cations on ExoN activity of NP-exo MOPV and NP-exo LCMV. RNA HP4 was incubated
547 with NP-exo MOPV or NP-exo LCMV for 0, 0.1, 5 and 30 minutes (min) in the presence of 5 mM
548 Mg^{2+} , Mn^{2+} , Zn^{2+} , Ca^{2+} , or EDTA. Digestion products were separated on a 20 % denaturing PAGE
549 and revealed by autoradiography. (B) Comparative mutational analysis of ExoN activity. The
550 DEDDh residues were mutated to alanine. Equal amounts of wild type (WT) or mutants of NP-exo
551 MOPV or NP-exo LCMV were incubated with HP4 for 0, 5 and 30 mins. Products were separated
552 on denaturing PAGE and visualized by autoradiography. NC indicates the substrate without
553 proteins. Sketch on the top of figure A illustrates the hairpin structure of HP4. On the side of each
554 gel is presented the migration size ladder in nucleotides (nts).

555 **Fig 2. Effect of divalent-Cation on thermal stability of NP-exo MOPV and NP-exo LCMV.** Bar
556 chart showing the shifts in melting temperatures of NP-exo MOPV and NP-exo LCMV measured in
557 the presence of 5 mM of the indicated ions by TSA.

558 **Fig 3. Comparison of the substrate on the ExoN activity of NP-exo MOPV and NP-exo LCMV.**
559 Comparative ExoN activity on three different RNA substrate ; A30 (ssRNA), LE19 (ssRNA forming
560 three types of secondary structures), HP4 (stable RNA hairpin). Equal amounts of each RNA
561 substrate were incubated with NP-exo MOPV or NP-exo LCMV for 0, 5, 30 minutes. Digestion
562 products were analyzed as in Fig1. On the side of each gel is presented the migration size ladder in

563 nucleotides (nts). A star highlight the enrichment of the band corresponding of a RNA of 17 nts
564 Type A RNA with degradation of 2 nucleotides.

565 **Fig 4. Time course hydrolysis of paired and mismatched 3'-end nucleotide base pair by NP-exo**
566 **MOPV and NP-exo LCMV.** (A) Schematic representation of dsRNA mimicking a replication
567 intermediate. RL2*/RT1, RL3*/RT1, RL4*/RT1 and RL5*/RT1 represent dsRNAs carrying either
568 zero, one, two and three non-complementary nucleotides respectively at their 3'-ends. (B) Equal
569 amounts of the dsRNA substrate (1,25 μ M) listed above were incubated in the absence or presence
570 of 0,25 μ M of NP-exo MOPV or NP-exo LCMV at 37 °C for 1, 2, 5 and 10 min. 0 is negative
571 control without proteins. A migration size ladder in nucleotides (nts) is presented on the side of the
572 gel. Digestion products were analyzed on 20% denaturing PAGE and visualized by
573 autoradiography. (C) Bar graph showing the total degradation product of substrate at various times.
574 Total degradation products were quantified using phosphoimager FLA-3000 (Fuji) and graphs
575 plotted using Graphpad. PRISM.

576 **Fig 5. Comparison of the ExoN domains : nsp14 SARScov and NP-exo MOPV.** Topology
577 diagrams of the (A) nsp14 SARScov and (B) NP-exo MOPV. The 5 β -strands that constitute the
578 central β -sheet are colored blue, pink, brown, yellow and green from the first to the fifth strand
579 respectively. The 4th and 6th α -helices of the DEDD motif are colored purple and orange
580 respectively. The uncolored spheres represent additional non-conserved secondary structures. The
581 location of the catalytic residues are indicated with red spheres. Extra domain insertions for each
582 ExoN are enclosed with in the large gray circles. The N and C terminals are indicated with the
583 uncolored squares. The topology diagrams indicates a similar fold and a conservation of the
584 catalytic core for both ExoNs. (C) Structural alignment of the active sites of nsp14 SARScov and
585 NP-exo MOPV. Color codes are same as in the topology diagrams except for secondary structures

586 colored cyan (NP-exo MOPV) or sandy brown (nsp14 SARScoV) which are not a part of the
587 catalytic fold. The superposition shows that catalytic residues are located at virtually identical
588 positions.

589 **Fig. 6. Effect of inactivated ExoN viruses on viral fitness and genome stability.** (A) Iterative
590 passages of NP-exo WT and D390A/G393A recombinant MOPV in Vero E6 cells. *De novo* stocks
591 of both viruses, from passage 1 to passage 10, were used to infect cells for 4 days with MOI 0.01.
592 Samples of supernatants were collected for viral infectious titration and NP RNA copy
593 quantification. Results for the left Y axis represent the infectious viral titers (FFU/mL) and results
594 from the right Y axis represent the NP RNA load (NP RNA copies/mL) of the corresponding cell
595 culture supernatants. (B) Ratio calculation for NP RNA copy load over infectious viral titer (RNA
596 copies / FFU) for NP-exo WT and D390A/G393A recombinant MOPV for the ten passages
597 considered in (A).

598 **Fig. 7. Representation of statistical occurrence of an amino acid at specific position.**
599 Represented the WebLogo of the corresponding MOPV amino acids S184, S1021 L1477 in all
600 Mammarenavirus, LASSV and MOPV sub set of sequences. The position of the residue of interest
601 is indicated with a red star. Size of the residue is proportional to its probability of occurrence (0 – 1).
602 For clarity, on the side of the WebLogo is the detailed statistical occurrence of all amino acids
603 found in the deposited sequences.

604 **Table 1. Observed L segment mutations of WT and ExoN(-) viruses at passages #1 and #10.**

605 **Supporting information**

606 **S1 Fig. Modular and organization of *Arenaviridae*' NP.** Schematic of the two domains
607 organization of *Arenaviridae*' NP, with its corresponding domains structures. N-terminal domain
608 corresponding to the nucleoprotein domain (PDB : 3T5N) and C-terminal domain corresponding to
609 the ExoN domain (PDB : 3Q7C) of LASV. Each domain is represented in ribbon and colored
610 following rainbow nomenclature from blue (N-terminus) to red (C-terminus). Flexible linker is
611 represented as green line.

612 **S2 Fig. Secondary structures adopted by RNA substrates used in the study.** (A) These
613 structures were predicted using Mfold server (<http://unafold.rna.albany.edu/?q=mfoldand>). The
614 minimum free energy of each structure is indicated below it. RNA HP4 is a stable RNA hairpin.
615 RNA LE19 presents 3 types of secondary structures. Type A : two double stranded nucleotides, type
616 B : long hanging 5' and short hanging 3' extremities, type C : long 5' 3' Hanging extremities. RNA
617 A30 long single stranded RNA without secondary structure. (B) Expected pattern of digestion based
618 on a dsRNA 3'5' ExoN activity for each type of tested RNA.

619 **S3 Fig. ExoN activity and divalent ion binding experiments of NP-exo MACV.** (A) Divalent-
620 cation dependent activity of NP-exo MACV. Protein was incubated with HP4 RNA in the presence
621 5 mM of Mn^{2+} , Mg^{2+} , Zn^{2+} or Ca^{2+} . The two last right lanes is a comparative time course hydrolysis
622 with two different RNA substrate ; A30 (ssRNA), LE19 (ssRNA forming secondary structures). NP-
623 exo MACV was incubated with equal amounts of each RNA substrate for 0, 5, 30 mins. Products
624 were separated on 20 % denaturing PAGE and visualized by autoradiography. (B) . Products were
625 analyzed as in A. (B) Change in melting temperature of NP-exo MACV in the presence of 5 mM of
626 mentioned ions measured by TSA.

627 **S4 Fig. Kinetics of HP4 cleavage by NP-exo MOPV WT, its Mutant D467A, NP-exo LCMV**
628 **WT or the corresponding mutant D459A.** HP4 was incubated with equal concentration of NP-exo
629 MOPV WT, D467A , NP-exo LCMV WT or D459A for 0, 2, 4, 6, 8, 10 and 15 mins. Reactions
630 products were separated on 20 % denaturing PAGE and products revealed by autoradiography. RNA
631 cleavage was then quantified from this data and plotted as the percentage of product formed with
632 time.

633 **S5 Fig. Structural alignment of 3'-5' ExoN :** (A) Ribbon representation of the superposition of
634 NP-exo Mopeia Virus (cyan pdb : 5LRP), nsp14 SARScov Exo (beige pdb : 5C8S), NP-exo Lassa
635 Virus (orange pdb : 4FVU), histone mRNA stem-loop by 3'-ExoN Homo Sapiens (green pdb
636 1ZBH). All structures were retrieved by PDBeFold (<http://www.ebi.ac.uk/msd-srv/ssm>), all similar
637 sequences were discarded. Overall fold is similar; in caption a zoom of the active site shows a quasi
638 perfect superimposition of the DEDD motif. Green spheres are in the zoom represent Mg ions. (B)
639 Weblogo of the active site derived from the structural alignment. Structure and sequence
640 comparison lead to conclude to a common origin of the ExoNs.

641 **S6 Fig. A model of the mechanism of calcium inhibition of 3'-5' ExoN activity.** (A) The dsRNA
642 from LASV NP-C structure (PBD code:4GV9) modeled into the MOPV Nexo-Mg structure.
643 MOPV-Mg represented as cartoon (Helices in orange, β -strands in green and loops in cyan) and the
644 dsRNA is shown as a stick model. The green balls represent magnesium atom. (B) An enlarged
645 view of the active indicating the model positions of ions during cleavage mechanism. Calcium
646 substitution of the magnesium ion mediates inhibition of 3'-5' ExoN activity as a result of its atomic
647 radius, binding flexibility and poor activation of water. Ca atom is represented in grey.

648 **S1 Table. Primer sequences used for mutagenesis of the LCMV and MOPV.**

649 **S2 Table. Oligomers names and sequences.**

650 **S3 Table. Comparison of remaining sequence length function of time.**

651 **S4 Table. Observed S segment mutations of WT and ExoN(-) viruses at passages #1 and #10.**

Figure 1

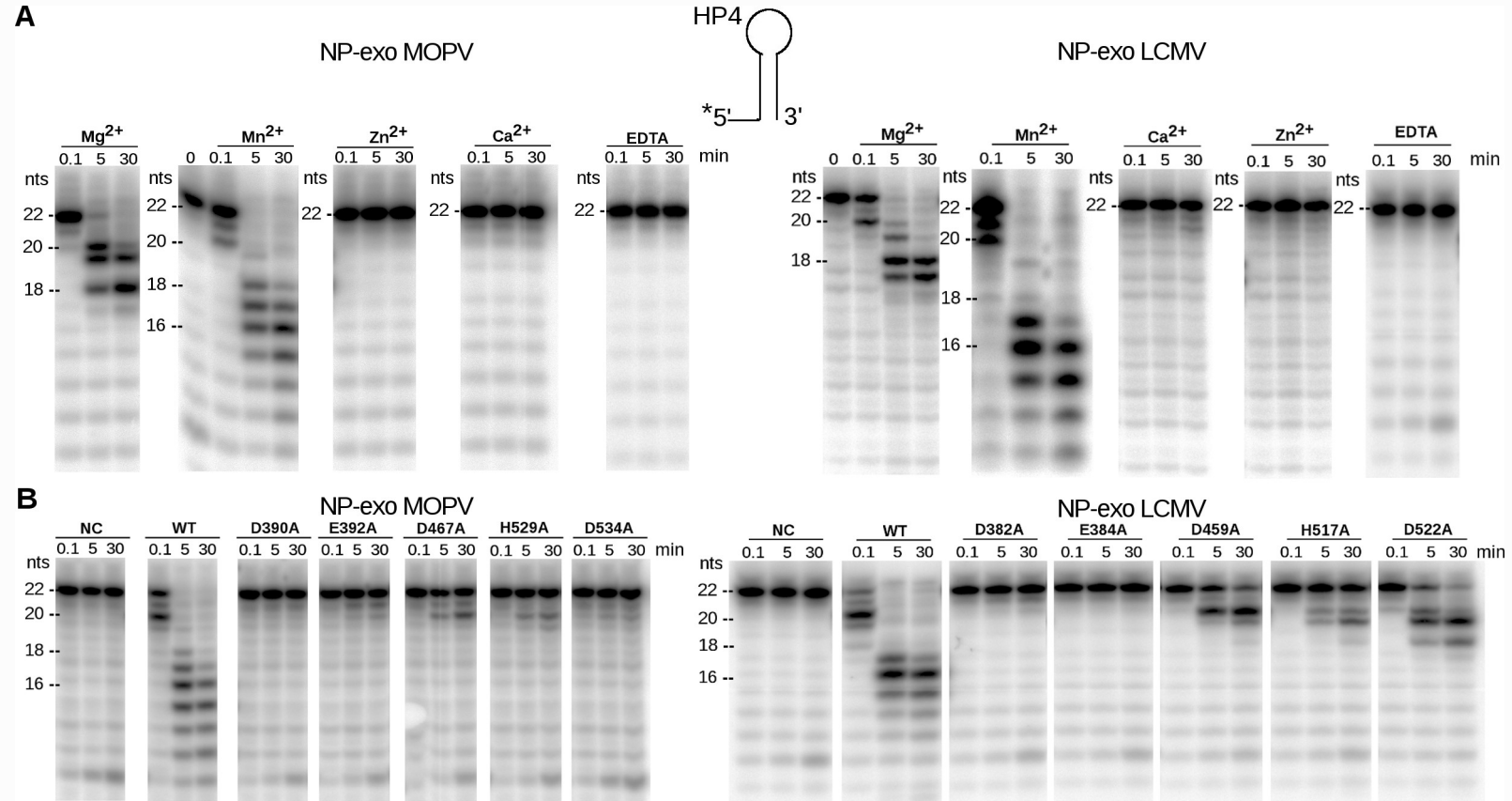


Figure 2

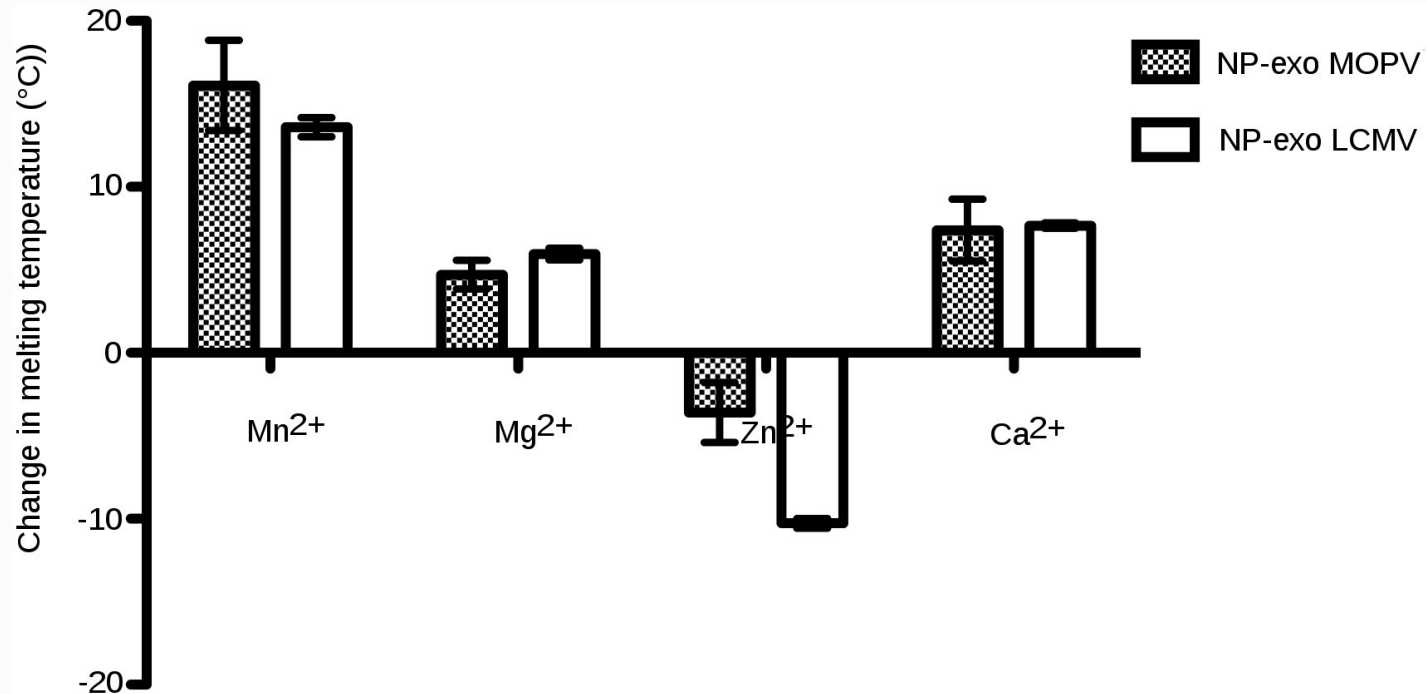


Figure 3

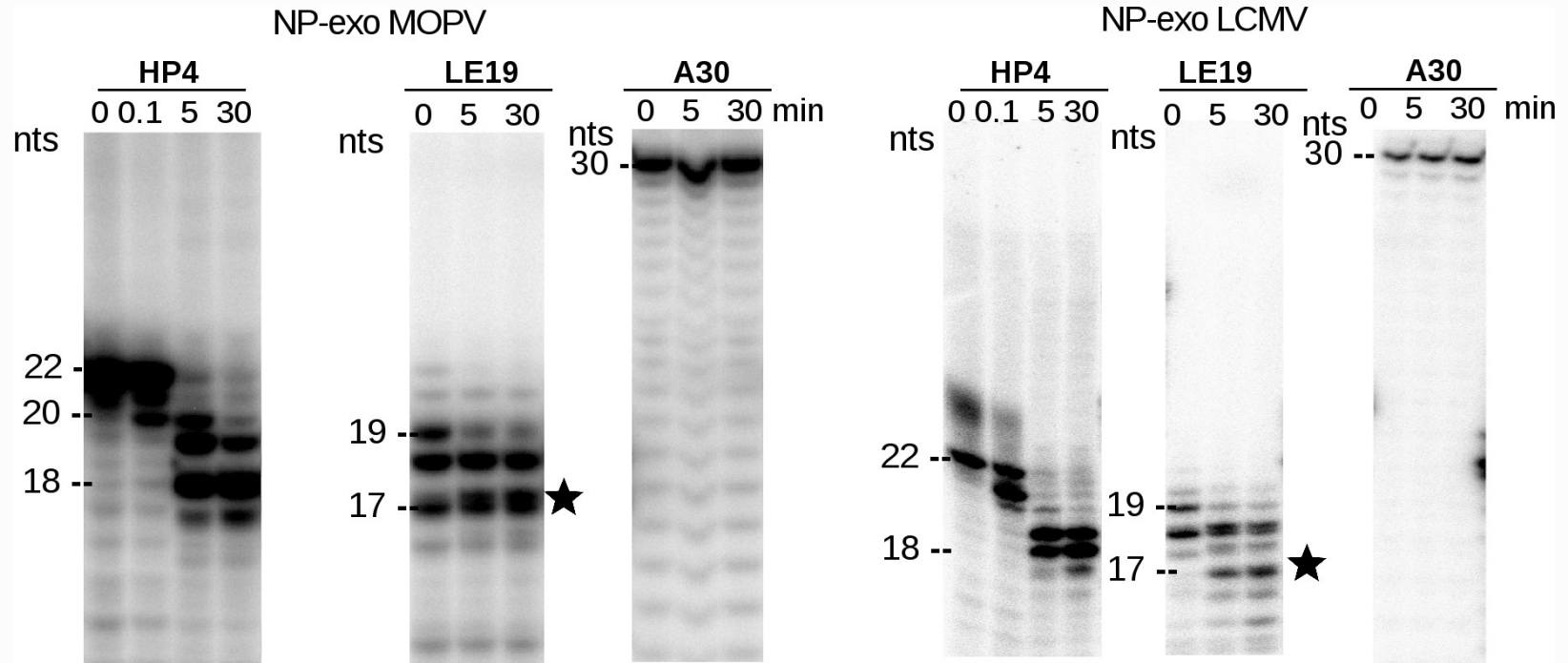


Figure 4

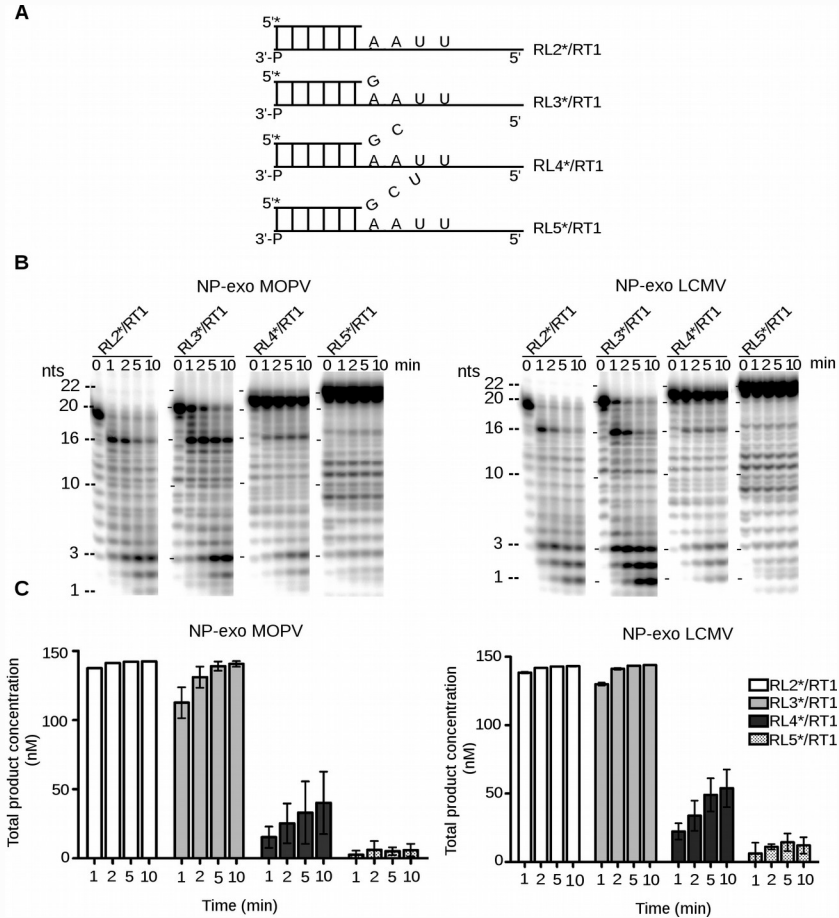
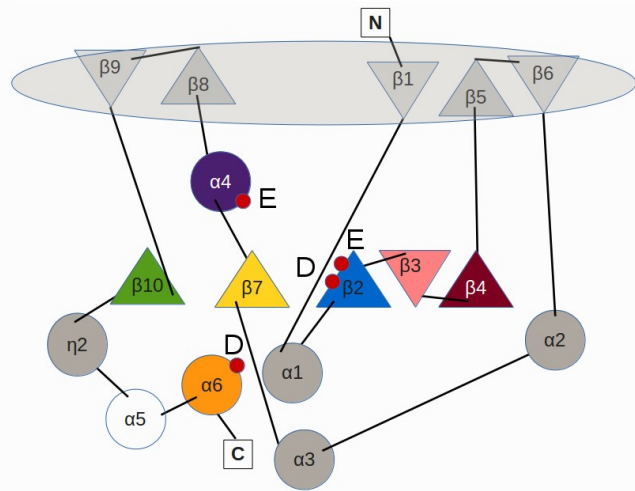
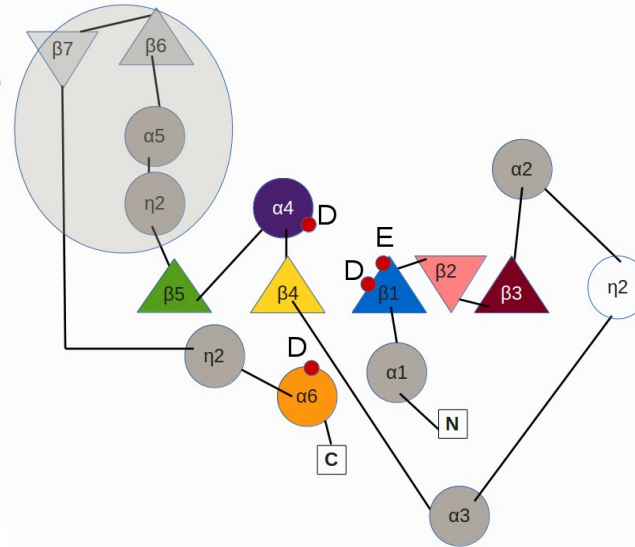


Figure 5

A



B



C

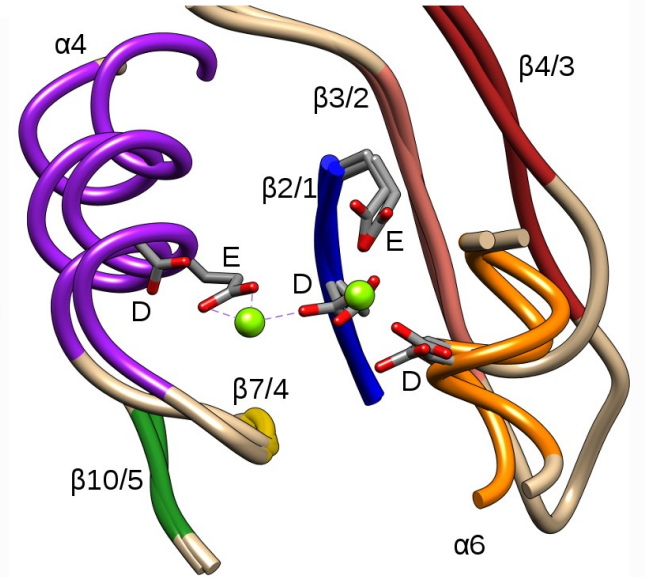
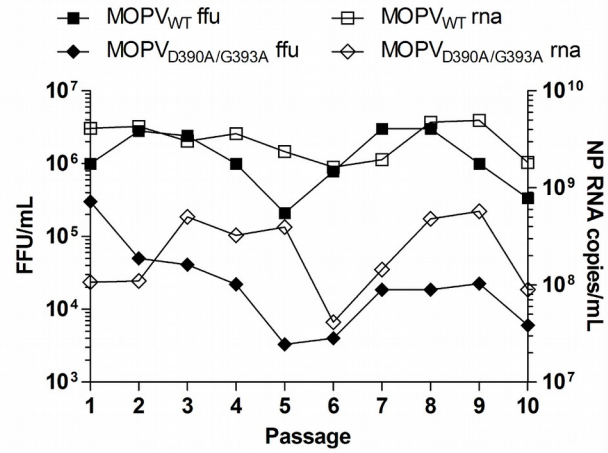


Figure 6

A



B

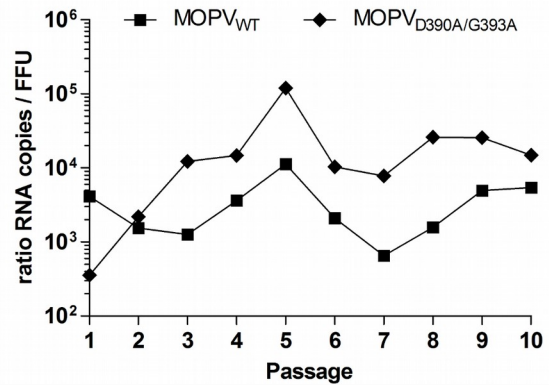
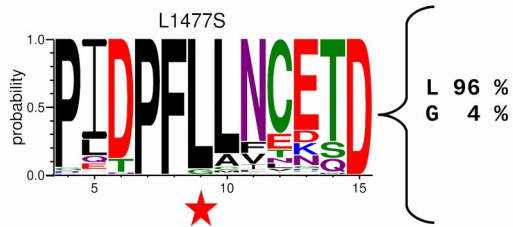
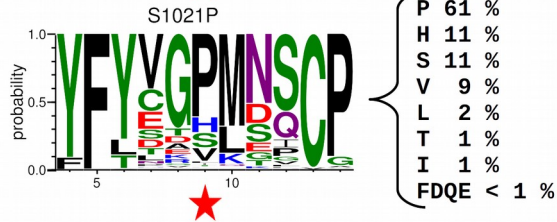
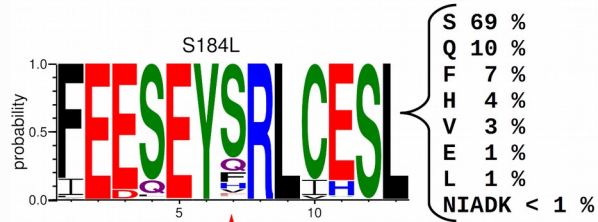
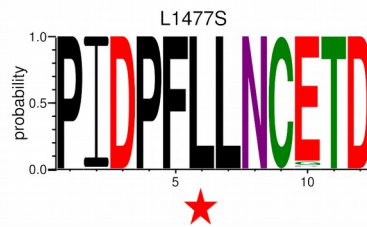
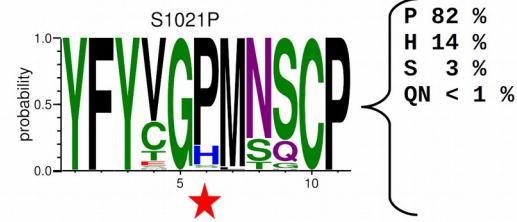
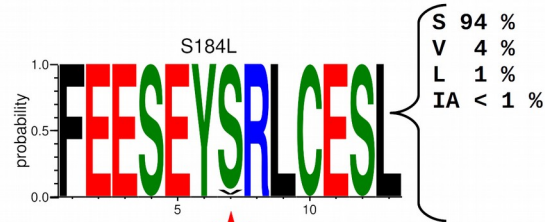


Figure 7

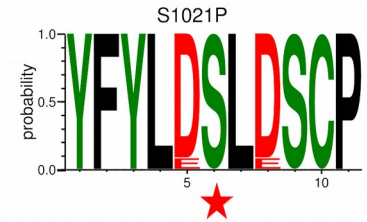
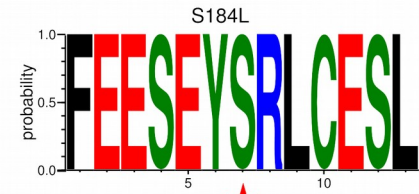
Mammarenavirus



Lassa Virus



Mopeia Virus



| | Passage #01 | | | | | |
|---------|-------------|-----|-----|--------|---------|-------------|
| | position* | ref | mut | region | residue | frequency % |
| MOPV WT | 9 | A | G | 5'UTR | | 12,500 |
| | 12 | A | G | 5'UTR | | 13,580 |
| | 742 | A | T | Lpol | M229L | 10,096 |
| | 1733 | T | C | Lpol | L559S | 6,140 |
| | 2463 | T | A | Lpol | F802L | 6,058 |
| | 2524 | A | G | Lpol | T824A | 6,043 |
| | 4473 | C | T | Lpol | P1471P | 12,058 |
| | 4663 | T | G | Lpol | L1536V | 11,227 |
| | 4691 | A | T | Lpol | K1545M | 6,941 |
| | 5471 | T | A | Lpol | V1805E | 9,798 |
| | 6251 | C | T | Lpol | P2065L | 8,235 |
| | 6259 | G | C | Lpol | D2068H | 9,002 |
| | 6452 | A | G | Lpol | E2132G | 9,379 |
| | 6564 | A | G | Lpol | G2169G | 6,528 |
| | 6746 | T | G | Lpol | V2230G | 18,750 |
| | 6903 | A | G | Z | N97N | 5,769 |
| | 7262 | T | G | 3'UTR | | 7,692 |

| Passage #10 | | | | | | |
|-------------|-----|-----|--------|-----------|-------------|--|
| position* | ref | mut | region | residue | frequency % | |
| 5 | A | G | 5'UTR | | 12,500 | |
| 9 | A | G | 5'UTR | | 6,122 | |
| 735 | T | C | Lpol | N226N | 5,430 | |
| 792 | T | C | Lpol | F245F | 6,667 | |
| 817 | A | G | Lpol | I254L | 25,411 | |
| 1024 | C | T | Lpol | H323Y | 7,478 | |
| 1097 | G | A | Lpol | R347K | 5,144 | |
| 1397 | G | A | Lpol | S447N | 6,585 | |
| 1834 | C | T | Lpol | P593S | 23,560 | |
| 2212 | T | G | Lpol | F719V | 6,263 | |
| 2233 | G | A | Lpol | D726N | 7,390 | |
| 2463 | T | A | Lpol | F802L | 7,765 | |
| 2840 | A | G | Lpol | D928G | 15,826 | |
| 3217 | C | T | Lpol | Q1054Stop | 5,810 | |
| 4498 | G | A | Lpol | D1480N | 5,200 | |
| 4868 | G | A | Lpol | S1604N | 8,793 | |
| 5407 | G | T | Lpol | A1784S | 24,272 | |
| 5422 | A | G | Lpol | R1789G | 16,089 | |
| 5992 | G | C | Lpol | V1979L | 6,454 | |
| 6024 | A | T | Lpol | S1989S | 8,835 | |
| 6268 | C | T | Lpol | P2071S | 8,788 | |
| 6302 | A | T | Lpol | D2082V | 12,893 | |
| 6406 | T | C | Lpol | F2117L | 5,393 | |
| 6602 | G | T | Lpol | R2182I | 10,453 | |
| 6769 | T | G | Lpol | Stop-E | 11,724 | |
| 6802 | C | T | IGR | | 9,524 | |
| 6965 | G | T | Z | P77S | 6,856 | |
| 6990 | C | A | Z | R68M | 11,690 | |
| 6992 | T | G | Z | D67D | 11,761 | |
| 7017 | A | T | Z | L59L | 7,450 | |
| 7020 | A | T | Z | C58C | 7,471 | |
| 7099 | C | A | Z | G32A | 7,673 | |

| | Passage #01 | | | | | |
|--------------|-------------|-----|-----|--------|---------|-------------|
| | position* | ref | mut | region | residue | frequency % |
| MOPV Exo (-) | 9 | A | G | 5'UTR | | 16,667 |
| | 12 | A | G | 5'UTR | | 12,121 |
| | 17 | A | G | 5'UTR | | 5,036 |
| | 742 | A | T | Lpol | M229L | 5,552 |
| | 2463 | T | A | Lpol | F802L | 5,583 |
| | 2518 | T | C | Lpol | L822L | 6,373 |
| | 6452 | A | G | Lpol | E2132G | 5,816 |
| | 6602 | G | T | Lpol | R2182I | 5,553 |
| | 6870 | C | T | IGR | | 12,903 |
| | 6990 | C | A | Z | R68M | 7,550 |
| | 6992 | T | G | Z | D67D | 7,462 |

| Passage #10 | | | | | | |
|-------------|-----|-----|--------|---------|-------------|--|
| position* | ref | mut | region | residue | frequency % | |
| 5 | A | C | 5'UTR | | 8,333 | |
| 5 | A | G | 5'UTR | | 8,333 | |
| 9 | A | G | 5'UTR | | 6,122 | |
| 129 | A | C | Lpol | K23N | 6,522 | |
| 608 | C | T | Lpol | S184L | 93,178 | |
| 1456 | A | T | Lpol | R467W | 24,704 | |
| 2079 | T | C | Lpol | D674D | 6,373 | |
| 2233 | G | A | Lpol | D726N | 6,045 | |
| 2427 | G | A | Lpol | V790V | 7,237 | |
| 2622 | T | C | Lpol | D855D | 9,348 | |
| 3118 | T | C | Lpol | S1021P | 58,105 | |
| 3163 | A | T | Lpol | T1036S | 5,868 | |
| 3624 | T | C | Lpol | N1189N | 8,228 | |
| 4487 | T | G | Lpol | L1477W | 10,772 | |
| 4500 | T | A | Lpol | D1480D | 5,134 | |
| 4883 | A | G | Lpol | L1477S | 60,227 | |
| 5239 | G | A | Lpol | E1728K | 8,367 | |
| 6302 | A | T | Lpol | D2082V | 6,604 | |
| 6567 | A | T | Lpol | R2169R | 9,287 | |
| 6729 | G | C | Lpol | R2225S | 9,980 | |
| 6769 | T | G | Lpol | Stop-E | 6,829 | |
| 6772 | G | A | IGR | | 9,596 | |
| 6870 | C | T | IGR | | 6,667 | |
| 6965 | G | T | Z | L76L | 6,655 | |
| 7032 | T | C | Z | L54L | 27,373 | |

* position number correspond to antigenome sens numbering

mutations present in both segments of the two viruses at passages 01 and 10

mutations present in one segment of both viruses at passage 10

non-synonymous mutations that became majority at passage 10

Table 1 : Observed mutation between WT and Mutant Exo (-) of segment L at passages #1 and #10.